ENERGY-DEPENDENT PROTON STOPPING AND DAMAGE FORMATION IN SULFUR-DOPED ZNO: A 3D ANALYSIS OF ELECTRONIC AND NUCLEAR ENERGY LOSS

Numonjonova Gulxayo Ismoiljon qizi
Andijan state university
Student of the Faculty of Physics, Mathematics and IT
Gmail: gulhayo88888@gmail.com
Phone number: +998947132823
Doniyorbekova Gulxayo Doniyorbek qizi
Gmail: gulxayodoniyorbekova@gmail.com
Phone number: +998955553112
https://doi.org/10.5281/zenodo.20505216

Abstract. This study investigates the energy-dependent stopping behavior and damage formation of protons in sulfur-doped zinc oxide (ZnO:S) using three-dimensional energy loss analysis. The obtained 3D profiles demonstrate that proton energy strongly influences both penetration depth and the dominant stopping mechanism in the ZnO:S matrix. High-energy protons penetrate deeper into the material, where energy dissipation is mainly governed by electronic stopping through interactions with target electrons. In contrast, low-energy protons deposit most of their energy near the surface region, where nuclear stopping becomes more pronounced due to elastic collisions with lattice atoms. This near-surface energy deposition leads to localized structural damage and the possible formation of radiation-induced defects. The comparative analysis of high- and low-energy proton irradiation reveals a clear transition from deep electronic energy loss to localized nuclear damage as proton energy decreases. These results provide important insight into the radiation response of ZnO:S and may be useful for optimizing ZnO-based materials for optoelectronic, sensor, space, and radiation-resistant applications.

Keywords: ZnO:S, proton irradiation, energy loss, electronic stopping, nuclear stopping, localized damage, 3D analysis.

Introduction. Zinc oxide (ZnO) is a promising wide-bandgap semiconductor material that has attracted considerable attention due to its unique optical, electrical, and structural properties. Owing to its high exciton binding energy, good chemical stability, transparency in the visible region, and compatibility with different doping elements, ZnO is widely considered for applications in optoelectronic devices, gas sensors, transparent conducting layers, ultraviolet photodetectors, and radiation-resistant electronic systems. The physical properties of ZnO can be effectively modified by impurity doping, which allows the tuning of its electronic structure, defect states, conductivity, and optical response. Among different dopants, sulfur incorporation into ZnO is of particular interest because sulfur can influence the lattice structure, band characteristics, and defect formation behavior of the host material. Sulfur-doped ZnO (ZnO:S) may exhibit modified electronic and optical properties compared with undoped ZnO due to changes in local bonding, oxygen-related defects, and impurity-induced states. These features make ZnO:S a potential candidate for advanced functional devices operating under different environmental and irradiation conditions. However, for practical use in space, nuclear, and high-radiation environments, it is important to understand how energetic particles interact with ZnO:S and how radiation-induced energy loss affects the stability of the material. Proton irradiation is one of the most important factors influencing the performance and reliability of semiconductor materials in radiation-rich environments.

When protons penetrate a solid target, they gradually lose their kinetic energy through interactions with target electrons and atomic nuclei. These two mechanisms are commonly known as electronic stopping and nuclear stopping. Electronic stopping is mainly associated with inelastic interactions between incident protons and electrons in the target material, while nuclear stopping is related to elastic collisions between protons and lattice atoms. The relative contribution of these two processes strongly depends on the incident proton energy. High-energy protons generally penetrate deeper into the material and lose most of their energy through electronic stopping. In this case, energy dissipation occurs over a relatively larger depth range, and the direct displacement damage to the crystal lattice is comparatively less localized. In contrast, low-energy protons have a shorter projected range and tend to deposit a significant part of their energy near the surface region. Under such conditions, nuclear stopping becomes more prominent, leading to enhanced atomic displacements, vacancy formation, interstitial defects, and localized structural damage. Therefore, the energy-dependent stopping behavior of protons is a key factor in determining the radiation response and defect evolution of ZnO:S. Three-dimensional visualization of proton energy loss provides a useful approach for analyzing the spatial distribution of deposited energy inside the material. Such analysis makes it possible to compare penetration depth, stopping intensity, and damage localization for different proton energies. In the present study, the energy-dependent proton stopping behavior in sulfur-doped ZnO is investigated using 3D energy loss profiles. Special attention is given to the transition from deep electronic stopping at high proton energies to near-surface nuclear stopping and localized damage at low proton energies. The obtained results provide important insight into the interaction of proton radiation with ZnO:S and contribute to the understanding of its potential radiation tolerance for optoelectronic, sensor, space, and radiation-resistant applications.

Materials and Methods

In the present work, the interaction of protons with sulfur-doped zinc oxide was investigated using a numerical ion–solid interaction approach. Sulfur-doped ZnO was considered as the target material because of its potential use in optoelectronic, sensing, and radiation-tolerant device structures. The target composition was defined as ZnO:S with atomic fractions of 48.0% Zn, 49.0% O, and 3.0% S. This composition was used to represent a sulfur-modified ZnO matrix in which proton-induced energy deposition and defect formation could be evaluated as a function of incident ion energy. The proton irradiation process was simulated using the SRIM/TRIM computational package. This software is based on the binary collision approximation and allows the calculation of ion trajectories, stopping power, projected range, recoil production, ionization losses, phonon losses, and vacancy formation in solid targets. Hydrogen ions were selected as incident particles, and their transport in the ZnO:S target was analyzed under different initial energy conditions. In order to compare shallow and deep irradiation regimes, four representative proton energies were selected: 10 keV, 100 keV, 500 keV, and 1000 keV. These energies make it possible to distinguish between near-surface damage dominated by low-energy protons and deeper penetration behavior associated with high-energy protons. The simulation geometry was arranged so that protons were incident on the surface of the ZnO:S target. During penetration, the ions gradually lose their kinetic energy through two principal mechanisms: electronic stopping and nuclear stopping. Electronic stopping corresponds to inelastic interactions between incident protons and target electrons, while nuclear stopping is related to elastic collisions with Zn, O, and S atoms in the lattice. The relative contribution of these two energy-loss channels was evaluated for each proton energy in order to determine the dominant mechanism of energy deposition. The SRIM output data were analyzed to

obtain depth-dependent distributions of energy loss and radiation damage. Particular attention was paid to ionization energy loss, phonon energy loss, recoil behavior, and vacancy generation. The ionization-related component was used to evaluate electronic energy dissipation, whereas vacancy and recoil distributions were considered as indicators of structural damage caused by nuclear collisions. The depth profiles obtained from the simulations were used to compare the spatial distribution of proton-induced effects at different energies. Three-dimensional energy loss maps were constructed to visualize the variation of stopping behavior inside the ZnO:S target. The color distribution in the 3D plots represents the relative intensity of energy loss, where higher values correspond to stronger energy deposition and a higher probability of radiation-induced damage. Damage formation was evaluated by considering vacancy production and the spatial localization of deposited energy. Regions with stronger nuclear stopping were interpreted as zones with a higher probability of atomic displacement, vacancy formation, and local lattice disorder. By comparing the calculated profiles at 10 keV, 100 keV, 500 keV, and 1000 keV, the transition from surface-localized damage to deeper electronic energy loss was determined. This methodology provides a basis for understanding the radiation response of sulfur-doped ZnO and for assessing its suitability for devices operating under proton irradiation conditions.

Results and Discussion

The SRIM-based analysis demonstrates that the interaction of protons with sulfur-doped ZnO strongly depends on the incident proton energy. The calculated stopping parameters show that proton energy controls not only the penetration depth, but also the dominant channel of energy dissipation inside the ZnO:S matrix. In all considered energy ranges, the electronic stopping component remains higher than the nuclear stopping component. However, their relative contribution changes significantly as the incident proton energy increases. At low proton energy, such as 10 keV, the projected range is limited to the near-surface region. In this case, the electronic stopping power is about 93 keV/μm, while the nuclear stopping power reaches 4.5 keV/μm. Although electronic stopping is still numerically larger, the nuclear contribution is more important for defect generation because low-energy protons transfer momentum more effectively to lattice atoms. Therefore, low-energy irradiation leads to stronger local atomic displacement and near-surface damage formation. As the proton energy increases to 100 keV, the electronic stopping power reaches its maximum value of about 212 keV/μm, whereas the nuclear stopping decreases to approximately 0.88 keV/μm. This indicates that protons in this energy region lose energy mainly through interactions with target electrons. The projected range also increases, showing that the deposited energy is distributed over a larger depth compared with 10 keV irradiation. For higher proton energies, particularly 500 keV and 1000 keV, the projected range increases considerably. At 500 keV, protons penetrate several micrometers into the ZnO:S matrix, while at 1000 keV the projected range reaches about 12 μm. In this energy region, nuclear stopping becomes very small, decreasing to nearly 0.10 keV/μm at 1 MeV. This means that high-energy protons mainly produce ionization rather than direct displacement of lattice atoms. Therefore, the probability of severe structural damage is reduced despite the deeper penetration of protons.

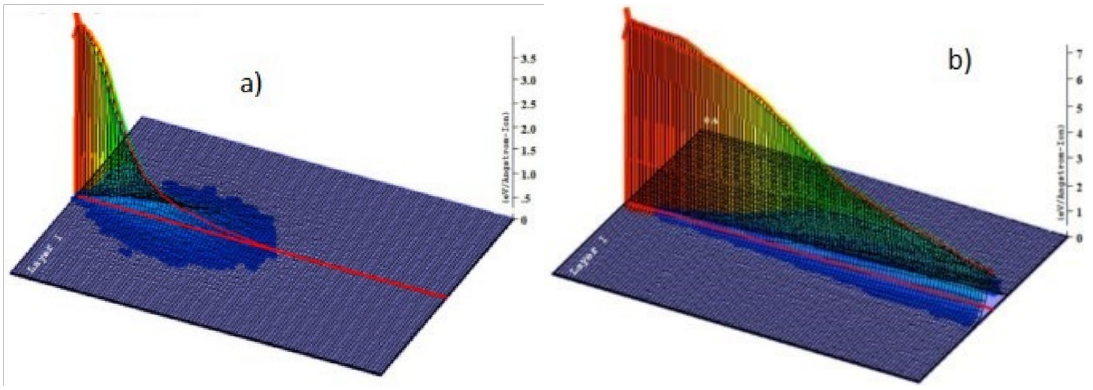

Fig. 1. Three-dimensional view of proton energy loss in sulfur-doped ZnO: (a) high-energy protons penetrate deeper into the ZnO:S matrix, with energy loss mainly governed by electronic stopping; (b) low-energy protons deposit most of their energy near the surface, where nuclear stopping becomes more pronounced and localized damage is formed.

As shown in Fig. 1, the energy loss behavior of protons in ZnO:S strongly depends on the incident proton energy. In the high-energy case, protons penetrate deeper into the material and lose their energy mainly through electronic interactions with the target electrons. This results in a broader and deeper energy deposition profile with comparatively weaker lattice damage. In contrast, low-energy protons deposit their energy within a shallow near-surface region. The localized high-intensity region indicates enhanced nuclear stopping, which increases the probability of atomic displacement, vacancy formation, and local structural disorder. Therefore, the 3D profiles clearly demonstrate the transition from deep electronic energy loss at high proton energies to localized nuclear damage at low proton energies.

The three-dimensional energy loss profiles provide a clear visualization of the difference between high- and low-energy proton irradiation regimes. In the case of high-energy protons, the energy loss is distributed along a deeper trajectory inside the ZnO:S target. The corresponding 3D surface shows a more extended energy deposition region, which is associated with dominant electronic stopping. Since high-energy protons interact mainly with the electron system of the target, the resulting energy loss is less localized and causes comparatively weaker lattice damage. In contrast, the 3D profile for low-energy protons shows that most of the energy is deposited close to the surface. The sharp and localized high-intensity region indicates that low-energy protons lose their energy over a short depth interval. This behavior is directly related to enhanced nuclear stopping, where elastic collisions between protons and Zn, O, and S atoms become more effective. At 10 keV, the damage profile is highly localized, and the vacancy concentration reaches its maximum within the first shallow layer of the material. This indicates that low-energy protons can be useful for controlled surface defect engineering. At 100 keV, the damage region becomes broader compared with 10 keV irradiation. The vacancy peak shifts deeper into the material, and the distribution becomes less sharp. This behavior suggests that increasing proton energy spreads the displacement events over a larger volume. Although vacancy formation still occurs, the damage is less concentrated than in the 10 keV case. For 500 keV and 1000 keV protons, the vacancy concentration decreases significantly. Even though these protons penetrate much deeper, their reduced nuclear stopping limits the formation of displacement defects. Therefore, high-energy proton irradiation produces a wider but more dilute damage profile. This result confirms that penetration depth alone does not determine the level of radiation damage; the nuclear stopping contribution is the key factor controlling vacancy generation. The ionization component increases with proton energy and becomes the dominant energy-loss process at high energies. This indicates that fast protons

primarily interact with the electronic subsystem of ZnO:S. Such interactions may lead to electron excitation and ionization, but they do not necessarily produce strong atomic displacement. Therefore, high-energy proton irradiation is expected to have a weaker influence on the crystal lattice compared with low-energy irradiation. Phonon-related energy loss remains much smaller than ionization loss over the investigated energy range. This shows that only a limited fraction of the incident proton energy is converted into lattice vibration and local heating. The small phonon contribution also supports the conclusion that the main difference between low- and high-energy irradiation is governed by the balance between nuclear stopping and electronic stopping. The dominance of ionization at high proton energies is favorable for applications where deep penetration is required without strong destruction of the crystal structure. On the other hand, when surface defect formation is desired, low-energy proton irradiation is more effective because it enhances nuclear collisions and produces localized structural disorder. The displacement per atom (DPA) analysis further confirms the energy-dependent nature of radiation damage in ZnO:S. At low proton energies, the DPA profile is sharply peaked near the surface due to efficient momentum transfer from protons to lattice atoms. This means that low-energy protons generate a high density of atomic displacements within a narrow depth region. At 10 keV, the DPA maximum is located close to the surface, corresponding to the short projected range of low-energy protons. When the energy increases to 100 keV, the DPA distribution becomes broader, and the maximum value decreases because the energy deposition is spread over a larger depth. For 500 keV and 1 MeV protons, the DPA values decrease further, indicating that high-energy protons are less efficient in producing atomic displacement damage. However, excessive vacancy formation at low energies may degrade carrier transport and increase defect-related recombination. High-energy protons, in contrast, penetrate deeper into the ZnO:S matrix and mainly lose energy through electronic stopping. Since their nuclear stopping component is small, they produce fewer displacement defects. Overall, the results show that proton energy is the main factor determining the balance between penetration depth, electronic energy loss, nuclear stopping, vacancy production, and DPA formation in ZnO:S. The transition from localized near-surface damage at low energies to deeper electronic energy dissipation at high energies provides useful guidance for designing ZnO:S-based optoelectronic, sensor, and radiation-tolerant devices.

Conclusion. In this work, the energy-dependent stopping behavior and damage formation of protons in sulfur-doped ZnO were investigated using three-dimensional energy loss analysis. The obtained results show that the interaction mechanism between incident protons and the ZnO:S target strongly depends on proton energy. At lower proton energies, energy deposition occurs mainly within the near-surface region, where nuclear stopping plays an important role in producing atomic displacements, vacancy formation, and localized lattice disorder. This indicates that low-energy proton irradiation is more effective for surface modification and defect engineering of ZnO:S. With increasing proton energy, the penetration depth of protons increases, while the contribution of nuclear stopping decreases. High-energy protons mainly lose their energy through electronic stopping, resulting in deeper energy dissipation and relatively weaker structural damage. The 3D energy loss profiles clearly confirm the transition from localized near-surface damage at low energies to deeper and more distributed electronic energy loss at high energies. The comparison of electronic and nuclear stopping, vacancy formation, and damage localization demonstrates that proton energy is a key parameter controlling the radiation response of ZnO:S. Low-energy irradiation can be used when controlled surface defect formation is required, whereas high-energy irradiation is more suitable for applications requiring deeper penetration with limited lattice

disruption. These findings provide useful insight for the design and optimization of ZnO:S-based optoelectronic, sensor, space, and radiation-tolerant devices.

Adabiyotlar, References, Литературы:

1.Ali, Z., Liu, F., Wang, Y., Rasool, H. G., Wang, F., & Haseeb, M. (2025). *Nuclear Engineering and Technology, 57*(8), 103570. https://doi.org/10.1016/j.net.2025.103570

2. Abraham, P., Shaji, S., Avellaneda, D. A., Aguilar-Martínez, J. A., & Krishnan, B. (2023). *Materials Today Communications, 35*, 105909. https://doi.org/10.1016/j.mtcomm.2023.105909

3. Ayoub, I., Kumar, V., Alshahrie, M. A., et al. (2022). *Nanotechnology Reviews, 11*(1), 575–619. https://doi.org/10.1515/ntrev-2022-0035

4. Boboev, A. Y., Ergashev, B. M., Yunusaliyev, N. Y., & Xotamov, M. M. (2025). *East European Journal of Physics, 2*, 292–296. https://doi.org/10.26565/2312-4334-2025-2-36

5. Boboev, A. Y., Makhmudov, K. A., Ibrokhimov, Z. M., Rafikov, A. K., Yunusaliyev, N. Y., & Ibrokhimov, S. K. (2025). *East European Journal of Physics, 2*, 436–440. https://doi.org/10.26565/2312-4334-2025-2-54

6. Boboev, A. Y., Maxmudov, X. A., Yunusaliyev, N. Y., Ergashev, B. M., Tojiboyev, G. G., & Abdulkhaev, F. A. (2025). *Journal of Ovonic Research, 21*(4), 481–493. https://doi.org/10.15251/JOR.2025.214.481

7. Carleer, B. (2018). *Journal of Physics: Conference Series, 1063*(1), 012001. https://doi.org/10.1088/1742-6596/1063/1/012001

8. Dong, Y., Tuomisto, F., Svensson, B. G., Kuznetsov, A. Y., & Brillson, L. J. (2010). *Physical Review B, 81*(8), 081201. https://doi.org/10.1103/PhysRevB.81.081201

9. Kumari, P., Srivastava, A., Sharma, R. K., Saini, A., Sharma, D., Tawale, J. S., & Srivastava, S. K. (2022). *Materials Today Communications, 32*, 103845. https://doi.org/10.1016/j.mtcomm.2022.103845

10. Kutliev, U., Karimov, M., Sadullaeva, B., & Otaboev, M. (2018). *COMPUSOFT: An International Journal of Advanced Computer Technology, 7*(4), 2749–2751. https://ijact.in/index.php/j/article/view/431/412

11. Lee, Y., Lee, H.-W., Park, S., Kim, J., & Lee, J. (2025). *Nano Convergence, 12*(1), 1–9. https://doi.org/10.1038/s41427-025-00234-2

12. Marques, C., Wrobel, F., Aguiar, Y., Michez, A., Boch, J., Saigné, F., García Alía, R., et al. (2024). *Eng, 5*(1), 319–332. https://doi.org/10.3390/eng5010021

13. Nandipati, G., Setyawan, W., Roche, K., Kurtz, R. J., & Heinisch, H. L. (2020). *Journal of Nuclear Materials, 542A*, 152402. https://doi.org/10.1016/j.jnucmat.2020.152402

14. Pakseresht, P., & Apte, S. V. (2019). *International Journal of Multiphase Flow, 113*, 16–32. https://doi.org/10.1016/j.ijmultiphaseflow.2018.12.012

15. Patra, B., Das, A., & Basak, D. (2024). *Physica B: Condensed Matter, 678*, 415745. https://doi.org/10.1016/j.physb.2024.415745